Available online at www.sciencedirect.com
SCIENCE DIRECT®
Chemical Physics Letters 386 (2004) 248–253
CHEMICAL PHYSICS LETTERS
www.elsevier.com/locate/cplett

Quantum ignition of intramolecular rotation by means of IR + UV laser pulses

Yuichi Fujimura [a], Leticia González [b,*], Dominik Kröner [b], Jörn Manz [b,*], Imed Mehdaoui [b], Burkhard Schmidt [c]

[a] Department of Chemistry, Graduate School of Science, Tohoku University, 980-8578 Sendai, Japan
[b] Institut für Chemie, Physikalische und Theoretische Chemie, Freie Universität Berlin, Takustrasse 3, D-14195 Berlin, Germany
[c] Institut für Mathematik II, Freie Universität Berlin, Arnimallee 2-6, D-14195 Berlin, Germany

Received 30 July 2003
Published online: 11 February 2004

Abstract

Quantum ignition of intramolecular rotation may be achieved as follows: first, a few-cycle infrared (IR) laser pulse excites the torsional vibration in an oriented molecule. Subsequently, a well-timed ultrashort ultraviolet (UV) laser pulse induces a Franck–Condon type transition from the electronic ground to the excited state with approximate conservation of the intramolecular angular momentum. As a consequence, the torsional motion is converted into a unidirectional intramolecular rotation, with high angular momentum ($\approx 100\hbar$). The mechanism is demonstrated by means of representative laser driven wave packets which are propagated on ab initio potential energy curves of the model system (4-methyl-cyclohexylidene)fluoromethane.

1. Introduction

Recently, the first quantum simulations have been carried out, demonstrating the ignition of unidirectional intramolecular rotations in chiral molecules by means of linearly polarized laser pulses in the infrared (IR) frequency domain [1–3]. This approach may serve as alternative to chemical, electrochemical or photochemical stimuli of molecular rotors [4–9], which is an important challenge in molecular engineering [10–13].

The design of efficient laser pulses for unidirectional intramolecular rotations may profit from techniques of laser control in ultrashort time domains [14–17]. In this Letter, we shall exploit our new method of laser control based on few cycle IR + ultraviolet (UV) pulses. As shown in [18], these pulses allow to create vibrational momentum in a selective molecular bond, and to exploit this momentum in order to break the bond by a transition from attractive to dissociative potential energy surfaces of the electronic ground and excited states, respectively. Here we suggest, by analogy, that few-cycle IR + UV laser pulses should create and transfer intramolecular angular momentum from torsional to rotational motions in electronic ground and excited states, respectively. The method will be demonstrated using representative laser driven wavepackets which are propagated on ab initio potential energy surfaces for the oriented model system, (4-methyl-cyclohexylidene)fluoromethane (4MCF).

The model and techniques are presented in Section 2, the results and the conclusion are in Sections 3 and 4, respectively.

2. Model and techniques

As a model system we propose the oriented chiral olefin 4MCF, shown in Fig. 1. The laser pulses should drive first its torsion and then the intramolecular rotation of the CHF fragment versus the 4-Me(C_6H_9) fragment along the dihedral angle ϕ. This torsion/rotation

* Corresponding authors. Fax: +49-30-83854792.
E-mail addresses: leti@chemie.fu-berlin.de (L. González), jmanz@chemie.fu-berlin.de (J. Manz).

0009-2614/$ - see front matter © 2004 Elsevier B.V. All rights reserved.
doi:10.1016/j.cplett.2004.01.070

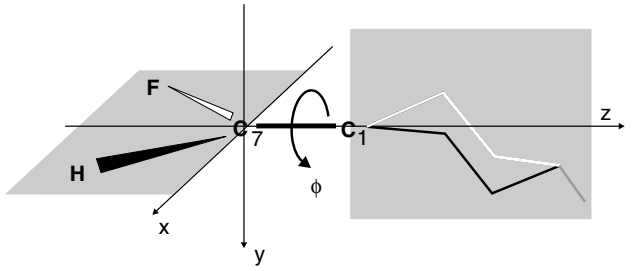

Fig. 1. The model system (4-methyl-cyclohexylidene)fluoromethane (4MCF). The molecular rotor is oriented such that the C=C double bond is along the z-axis, the y-z- plane serves as the mirror plane for the 4-Me(C_6H_9)-fragment, the intramolecular torsion/rotation of the CHF fragment is along the torsional angle ϕ. The figure shows the aR configuration ($\phi = 90°$). The arrow indicates the torsional rotational motion induced by the IR + UV laser fields.

is, in reduced dimensionality, described by the time-dependent Schrödinger equation:

$$i\hbar\frac{\partial}{\partial t}\begin{pmatrix}|\Psi_0(t)\rangle\\ |\Psi_1(t)\rangle\end{pmatrix} = \begin{pmatrix}\hat{\mathbf{H}}_{0,0}(t) & \hat{\mathbf{H}}_{0,1}(t)\\ \hat{\mathbf{H}}_{1,0}(t) & \hat{\mathbf{H}}_{1,1}(t)\end{pmatrix}\begin{pmatrix}|\Psi_0(t)\rangle\\ |\Psi_1(t)\rangle\end{pmatrix}, \quad (1)$$

where the labels 0 and 1 denote the adiabatic electronic ground (S_0) and excited singlet (S_1) states, respectively. Higher electronic excited states are neglected in the present model. In the adiabatic representation, the matrix elements of the Hamiltonian

$$\hat{\mathbf{H}}_{i,j}(t) = \hat{\mathbf{T}}_{i,j} + \hat{\mathbf{V}}_{i,j}\delta_{i,j} + \hat{\mathbf{W}}_{i,j}(t) \quad (2)$$

consist of contributions for the kinetic energy, potential energy, and for the laser–dipole coupling. The kinetic operator diagonal terms are given by

$$\hat{\mathbf{T}}_{00} = \hat{\mathbf{T}}_{11} = \hat{\mathbf{T}} = -\frac{\hbar^2}{2I}\frac{\partial^2}{\partial\phi^2}, \quad (3)$$

where I denotes the reduced torsional moment of inertia $I = 167396 m_e a_0^2$, whereas the off-diagonal terms $\hat{\mathbf{T}}_{01}$ and $\hat{\mathbf{T}}_{10}$ represent the non-Born–Oppenheimer or non-adiabatic couplings; these are not taken explicitly into account in the adiabatic limit calculations, but their effects will be discussed in Section 3. The adiabatic unrelaxed potential energy surfaces $V_0 \equiv V_{00}$ and $V_1 \equiv V_{11}$ along ϕ, shown in Fig. 2, are taken from [19], and they have been calculated using density functional theory (DFT) and its time-dependent version (TD-DFT), respectively, at B3LYP/6-311+G(d,p) level of theory. V_0 is a symmetric double well potential supporting two equivalent aS and aR enantiomers of the chiral olefine located at $\phi = -90°$ and $\phi = +90°$, respectively.

In the following, we shall consider model systems which are prepared initially as a pure enantiomer, e.g. the aR enantiomer, in its torsional ground state; pure enantiomers can be prepared from its racemate in different manners, for instance, by introducing a chiral catalyst which drives the reaction towards a single enantiomer (see [20–22]) or by means of external laser fields

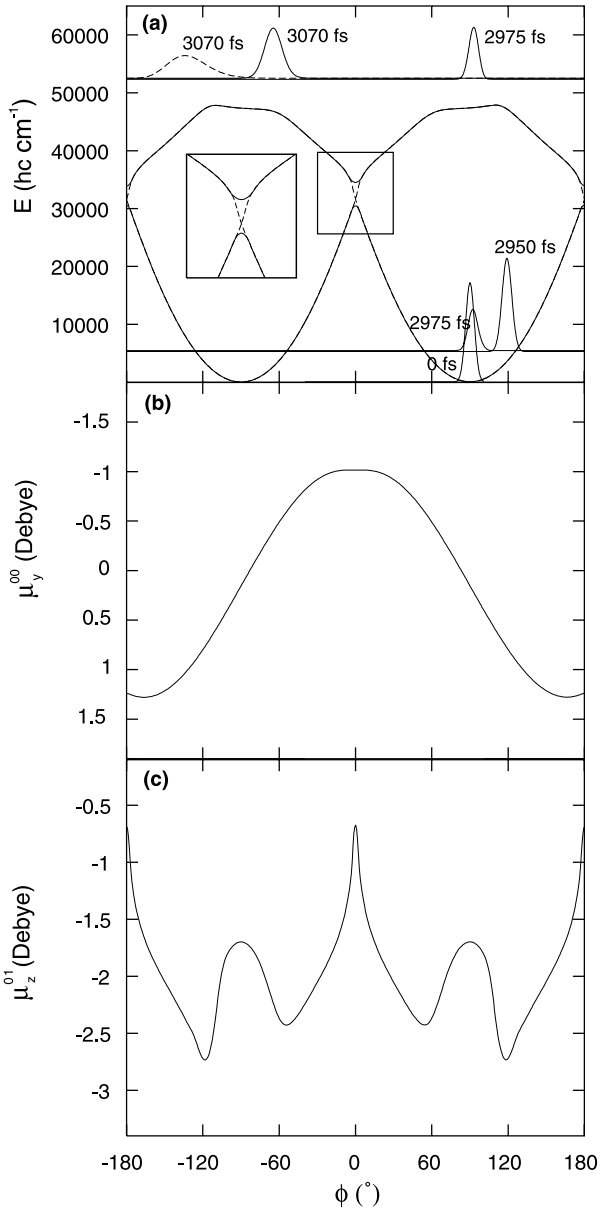

Fig. 2. Quantum ignition of the molecular rotor 4MCF simulated by laser driven wave packets. (a) Snapshots of the densities of the wave packet $\Psi_0(\phi,t)$ and $\Psi_1(\phi,t)$ moving on the adiabatic (solid) or diabatic (dashed) potential energy surfaces V_0 and V_1 with energies indicated by the horizontal lines. (b) Y-component of the permanent dipole moment that couples the IR field. (c) Z-component of the transition dipole moment that couples the UV field.

(see. e.g. [19]). In 4MCF, each enantiomer is well separated from the opposite one by two high potential energy barriers of the order of 30 000 hc cm^{-1} located at $\phi = 0°$ and $\phi = \pm 180°$. Likewise, V_1 is a symmetric double barrier potential with two minima located at $\phi = 0°$ and $\phi = \pm 180°$. The rather narrow energy gaps between the minima of V_1 and the maxima of V_0 suggest avoided crossings corresponding to diabatic potentials $\tilde{V}_1 \equiv \tilde{V}_{11}$ and $\tilde{V}_2 \equiv \tilde{V}_{22}$, which cross at $\phi = 0°$ and $\phi = \pm 180°$; for

further details about the topology of V_1 and higher excited potential energy surfaces, see [19]. The diabatic $\tilde{V}_1$ and $\tilde{V}_2$ are also indicated in Fig. 2, and they are constructed by linear interpolation of the adiabatic potentials V_1 and V_2, and by setting $\tilde{V}_1 \approx V_1$ or V_2 and $\tilde{V}_2 \approx V_2$ or V_1 in the domains of the aR ($10° \leqslant \phi \leqslant 170°$) and aS ($-170° \leqslant \phi \leqslant -10°$) enantiomers, respectively.

The laser–dipole interactions are given by

$$\hat{\mathbf{W}}_{i,j}(t) = -\vec{\mu}^{ij} \cdot \vec{E}(t), \tag{4}$$

with dipole operators $\vec{\mu}^{00}(\phi)$ and $\vec{\mu}^{11}(\phi)$ for the adiabatic electronic ground and excited states, and transition dipole operators $\vec{\mu}^{01}(\phi) = \vec{\mu}^{10}(\phi)$. The relevant components for the laser induced dynamics, i.e. $\vec{\mu}_Y^{00}(\phi)$ and $\vec{\mu}_Z^{01}(\phi)$ are also shown in Fig. 2 [19]. Note that $\vec{\mu}_Z^{01}(\phi)$ coincides with the corresponding $\tilde{\mu}_Z^{01}(\phi)$ in the diabatic representation whereas, the relations $\tilde{\mu}_Y^{00}(\phi) \approx \mu_Y^{00}(\phi)$ or $\mu_Y^{11}(\phi)$, hold in the domains of the aR and aS enantiomers, respectively. (The values of $\tilde{\mu}_Y^{00}(\phi)$ in the domains $-180° \leqslant \phi \leqslant 10°$ and $170° \leqslant \phi \leqslant 180°$ are irrelevant for the present application.) The electric field $\vec{E}(t)$ is designed as a sequence of intense linearly polarized few cycle IR + UV laser pulses

$$\vec{E}(t) = \vec{E}_{\mathrm{IR}}(t) + \vec{E}_{\mathrm{UV}}(t), \tag{5}$$

where

$$\begin{aligned}\vec{E}_k(t) &= \vec{\epsilon}_k \cdot E_k(t) \\ &= \vec{\epsilon}_k \cdot E_k^0 \cos(\omega_k \cdot (t - t_{d_k}) + \eta_k) \cdot s_k(t),\end{aligned} \tag{6}$$

with polarizations $\vec{\epsilon}_k$, amplitudes E_k^0, carrier frequencies ω_k, time delays t_{d_k}, phases η_k and shape functions $s_k(t)$ for k = IR or UV. For convenience, we employ

$$s_k(t) = \sin^2\left(\frac{\pi(t - t_{d_k})}{t_{p_k}}\right) \quad \text{for} \quad t_{d_k} \leqslant t \leqslant t_{d_k} + t_{p_k}, \tag{7}$$

$$s_k(t) = 0 \quad \text{else} \tag{8}$$

with total pulse durations t_{pk}. Moreover, for the forthcoming application, we use the parameters $\vec{\epsilon}_{\mathrm{IR}} = \vec{\epsilon}_Y$, $t_{d\mathrm{IR}} = 0$, and $\vec{\epsilon}_{\mathrm{UV}} = \vec{\epsilon}_Z$, and $t_{d\mathrm{UV}} > t_{p\mathrm{IR}}$, i.e. the IR and UV laser pulses are Y- and Z-polarized, respectively, and they do not overlap. The field amplitudes of the pulses used for quantum ignition correspond to maximum intensities $I_{\max,\mathrm{k}} = \varepsilon_0 \cdot c \cdot |\overline{E}_k^0|^2$; the field amplitudes E_{IR}^0 and E_{UV}^0 are chosen such that both $I_{\max,\mathrm{IR}}$ and $I_{\max,\mathrm{UV}}$ are below the Keldish limit for ionisation [23].

The time-dependent Schrödinger equation for the adiabatic potentials is propagated by means of the split-operator method [24–27] and the fast Fourier Transform method [28] with periodic boundary conditions, as implemented in the program package *Wavepacket* [29]. The initial values are given by

$$\begin{pmatrix} |\Psi_0(t=0)\rangle \\ |\Psi_1(t=0)\rangle \end{pmatrix} = \begin{pmatrix} |\chi_{0,aR}\rangle \\ 0 \end{pmatrix}, \tag{9}$$

where $|\chi_{0,aR}\rangle$ denotes the torsional ground state of the aR enantiomer, which is localized in the corresponding aR potential well. The corresponding torsional eigenfunctions are evaluated by means of the Fourier Grid Hamiltonian method [30]. The time-dependent densities in the adiabatic states $i = 0$ and 1 are given by

$$\rho_i(\phi, t) = |\langle\phi|\Psi_i(t)\rangle|^2 \tag{10}$$

and their populations P_i(t) are obtained as

$$P_i(t) = \int_{-\pi}^{\pi} \rho_i(\phi, t)\,\mathrm{d}\phi. \tag{11}$$

Complementary to the results for the time-dependent Schrödinger Eq. (1) in the adiabatic representation, we shall also present the results for the time-dependent Schrödinger equation

$$i\hbar\frac{\partial}{\partial t}\begin{pmatrix} |\tilde{\Psi}_0(t)\rangle \\ |\tilde{\Psi}_1(t)\rangle \end{pmatrix} = \begin{pmatrix} \tilde{\mathbf{H}}_{0,0}(t) & \tilde{\mathbf{H}}_{0,1}(t) \\ \tilde{\mathbf{H}}_{1,0}(t) & \tilde{\mathbf{H}}_{1,1}(t) \end{pmatrix}\begin{pmatrix} |\tilde{\Psi}_0(t)\rangle \\ |\tilde{\Psi}_1(t)\rangle \end{pmatrix}, \tag{12}$$

based on the diabatic representation, i.e.

$$\tilde{\mathbf{H}}_{i,j}(t) = \tilde{\mathbf{T}}_{i,j}\delta_{i,j} + \tilde{\mathbf{V}}_{i,j} + \tilde{\mathbf{W}}_{i,j}(t), \tag{13}$$

with diagonal kinetic energy operators $\tilde{\mathbf{T}}_{i,i} = \hat{\mathbf{T}}$, (cf. Eq. (3)), and the diabatic potentials and dipole couplings as discussed above, cf. Fig. 2. The off-diagonal diabatic potential couplings $\tilde{V}_{01} = \tilde{V}_{10}$ are neglected in the diabatic limit. The results for the solution of Eq. (1) or (12) then correspond to two limiting cases: the perfectly adiabatic or the perfectly diabatic molecular dynamics, implying 0% or 100% curve crossing at the avoided crossing of the adiabatic potentials, respectively. These limits should serve as references for the dynamics with probabilities of curve crossings between such limits.

3. Results

The ultrashort IR + UV laser fields are shown in Fig. 3a, and their effects on the aR-enantiomer are demonstrated in Figs. 2a and 3b–d. Due to the strong harmonicity of the potential wells, the IR pulse induces a coherent torsion of the CHF moiety of 4MCF in the electronic ground state by ladder climbing [31]. The corresponding torsional wave packet $\Psi_0(\phi, t)$ oscillates then around the equilibrium value $\langle\phi\rangle = 90°$, with increasing amplitudes between 54° and 126° (see Fig. 3b). Simultaneously, the torsional angular momentum oscillates (with $\pi/2$ phase shift) around the equilibrium value $\langle l_z\rangle = 0\hbar$, with increasing amplitude (see Fig. 3c). As seen in Fig. 2a , at the end of the IR laser pulse, the wave packet has been coherently shifted from the equilibrium position at $\langle\phi\rangle = 90°$ to the turning point ($\langle l_z\rangle = 0\hbar$) located at $\langle\phi\rangle = 126°$. Then, it swings back towards the opposite turning point at $\langle\phi\rangle = 54°$, thus gaining maximum torsional angular momentum,

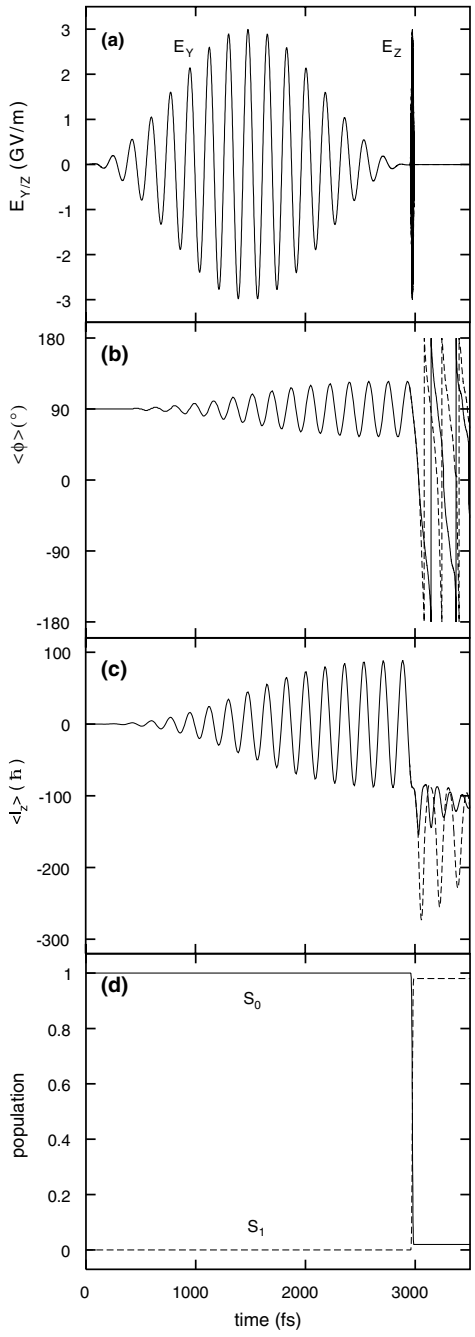

Fig. 3. Quantum ignition of the molecular rotor 4MCF simulated by laser driven wave packets. (a) IR and UV laser pulses. The IR field has parameters: $E^0_{\mathrm{IR}} = 3$ GV/m, ($I_{\max,\mathrm{IR}} = 2.39$ TW/cm^{-2}), $\omega_{\mathrm{IR}} = 189.15$ cm^{-1}, $t_{p\mathrm{IR}} = 2950$ fs and $\eta_{\mathrm{IR}} = 0$. The UV field has parameters: $E^0_{\mathrm{UV}} = 3$ GV/m, $\omega_{\mathrm{UV}} = 47100$ cm^{-1}, $t_{p\mathrm{UV}} = 40$ fs, $\eta_{\mathrm{UV}} = 0$, and $t_{d\mathrm{UV}} = 2955$ fs. (b) Time evolution of the mean torsional (before the UV pulse) and rotational (after the UV pulse) angle ϕ. Solid and dashed lines represent adiabatic and diabatic representations, respectively. (c) Time evolution of the mean angular momentum. Solid and dashed lines are like in (c). (d) Time evolutions of the populations in the electronic ground state (solid) and singlet excited state, S_1 (dashed).

$\langle l_z\rangle \approx 100\hbar$ as it passes through the equilibrium potential well of V_0 (cf. Fig. 3b and c). At this moment ($t = 2975$ fs), the ultrashort UV laser pulse has the maximum amplitude (Fig. 3a), and the wave packet $\Psi_0(\phi, t)$ is transferred nearly vertically from the electronic ground state to the excited singlet state with almost 100% efficiency (see Fig. 3d). As a consequence, the wave packet created in the V_1 state, $\Psi_1(\phi, t)$, possesses the same torsional angular momentum as in the V_0 state ($\langle l_z\rangle \approx 100\hbar$). The associated kinetic energy is large enough, such that subsequently, the wave packet $\Psi_1(\phi, t)$ moves along ϕ in a unidirectional manner (here towards smaller values of ϕ), overcoming all potential barriers of V_1 (see Fig. 2a). Close inspection of $\Psi_1(\phi, t)$ shows that the wave packet is slightly accelerated or slowed down as it runs down or climbs the potential slopes of V_1, respectively. As a consequence, the mean angular momentum $|\langle l_z\rangle| \approx 110\hbar$ even exceeds the value transferred by the UV pulse ($\approx 100\hbar$).

The preceeding results have been obtained for the limit of perfectly adiabatic wave packet dynamics. The results for the case of perfectly diabatic wave packet dynamics are also collected in Fig. 3b and c. Obviously, both types of wave packet dynamics agree until the wave packet reaches the avoided-crossing at $\phi = 0°$. Subsequently, the adiabatic wave packet $\Psi_1(\phi, t)$ moving on V_1 is slower than the diabatic one $\tilde{\Psi}_1(\phi, t)$ moving on $\widetilde{V_1}$, due to the deeper wells of $\tilde{V}_1$ compared to those of V_1. Clearly, the faster diabatic wave packet rotates with even larger torsional angular momentum values ($\approx 180\ \hbar$) than the adiabatic one. These limits of adiabatic vs. diabatic dynamics serve as a reference for the intermediate cases, $110\hbar \leqslant |\langle l_z\rangle| \leqslant 180\hbar$.

4. Conclusions

The present model simulations demonstrate that quantum ignition of unidirectional intramolecular rotation is possible in two steps: first, a few-cycle intense IR laser pulse excites the torsional motion of one molecular fragment against the rest of the molecule; second, a well-timed ultrashort UV laser field transfers the system from the electronic ground state into an excited state such that the torsional motion is converted into unidirectional intramolecular rotation. The second step exploits approximate conservation of torsional and intramolecular angular momentum in a near-vertical Franck–Condon type of transition.

In summary, the IR + UV laser fields serve to create torsional angular momentum and convert it into unidirectional rotational angular momentum, respectively. These effects are analogous to the creation and transfer of vibrational momentum which is used to induce selective bond breaking in e.g. HOD by means of intense few cycle IR + UV fields [18]. The present mechanism shares some common aspects with those of the group of Feringa and co-workers [5]; in particular, the present path from the configuration of the aR enantiomer to the

aS enantiomer is analogous to the *cis–trans* isomerization of [5]. Their isomerization is driven by incoherent vis (UV) light, and thermal energy is applied to prevent reversal rotation. In contrast, the present mechanism achieves unidirectionality by means of coherent IR laser pulses. Obviously, the directionality of the molecular rotor can be controlled e.g. by choosing appropriate time delays of the UV laser relative to the phase of the torsion induced by the IR field.

Quantum ignition of an intramolecular rotation may be exploited as initial step in order to drive a molecular rotor by laser light. After that, the unidirectional rotation has to be maintained in an efficient way such that a molecular machine could work. By analogy to macroscopic or biological machines, this second task requires permanent supply of energy. The most primitive solution to this problem is permanent repetition of the sequential IR + UV laser pulses, corresponding to perpetual re-start

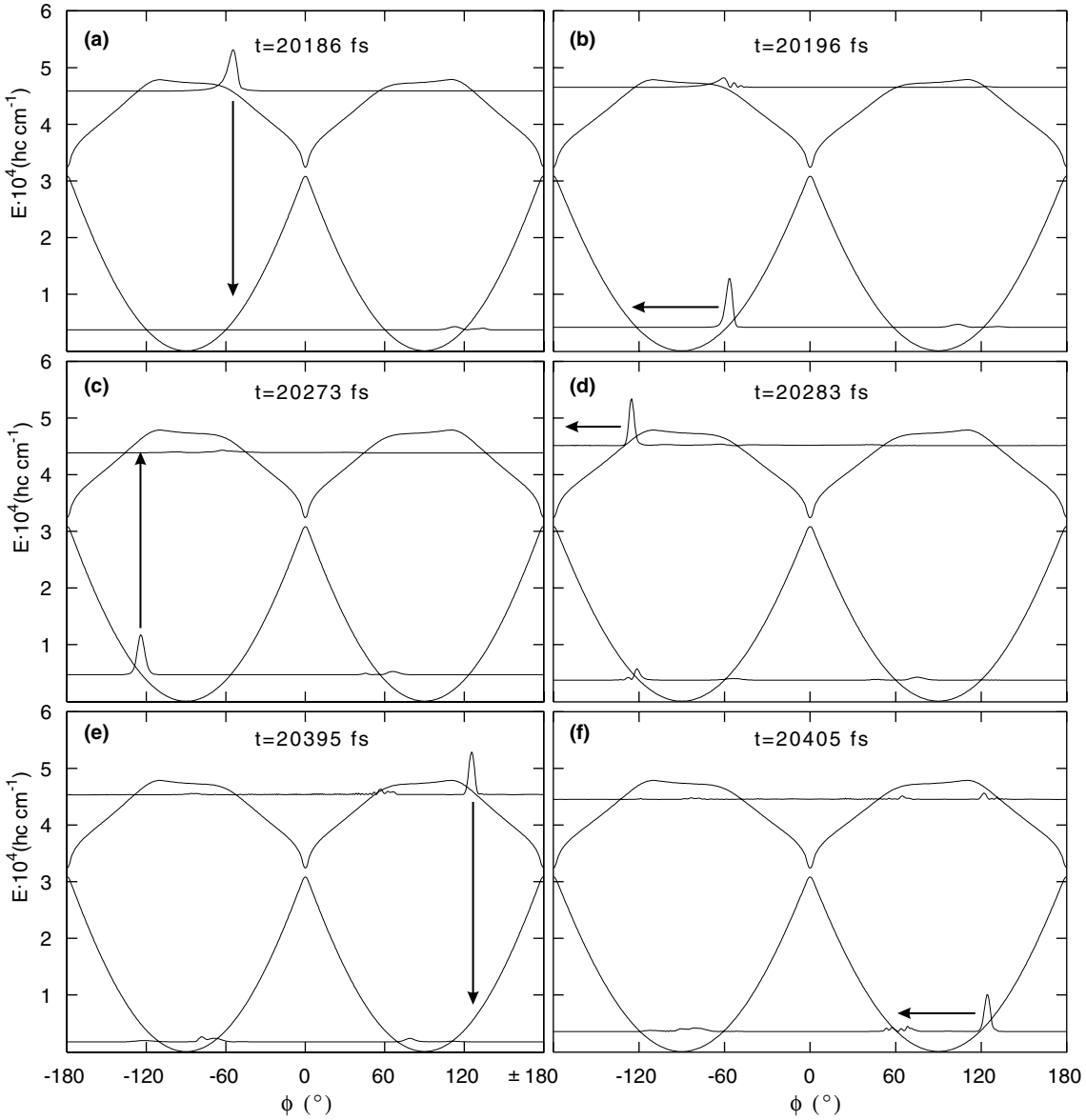

Fig. 4. Maintainance of unidirectional intramolecular rotation after quantum ignition by a series of ultrashort UV laser pulses. The model simulation shows the effects of laser pulses ($E^0_{UV} = 8.4$ GV/m, $\omega_{UV} = 40625$ cm^{-1}, $t_{pUV} = 10$ fs, $\eta_{UV} = 0$) fired at times, $t_2 = 20186$ fs, $t_3 = 20273$ fs, $t_4 = 20395$ fs on the rotational wavepackets $\Psi_0(t)$ and $\Psi_1(t)$, which are illustrated by snapshots of the the corresponding densities embedded in the potential energy surfaces V_0 and V_1 of the electronic ground and excited states, respectively. The base lines of these wavepackets indicate their mean potential energies. Specifically, snapshot a) shows the situation as prepared by IR + UV quantum ignition, at the time $t = 20186$ fs where the dominant part of the wavepackets is in the attractive domain of the electronic excited state and with total energy below the potential barrier of V_1, such that the original intramolecular rotation would be 'trapped' as torsional motion in the electronic excited state. Nevertheless, the unidirectional intramolecular rotation is maintained due to the sequential dump-pump-dump-etc UV laser pulses which induce well-timed transitions from attractive to repulsive domains of the potential energy surfaces in the electronic ground and excited states.

of the molecular rotor. A more efficient scheme is indicated by the mechanism illustrated in Fig. 4: After ignition of the unidirectional intramolecular rotation, it is maintained by a series of ultrashort UV pulses which induce sequential electronic transitions between the electronic ground and excited states. These pulses are well timed such that whenever the wavepacket representing rotational motions slows down due to attractive forces of the present domain of the potential energy surface, e.g. in the electronic excited state, it is re-accelerated by a transfer to the corresponding repulsive domain of the other potential energy surface, e.g. in the electronic ground state, and vice versa. Another possibility of maintaining unidirectional intramolecular rotations even in dissipative environments is implied by the approach of Korolkov and Paramonov [32], i.e. dissipative loss of rotational energy and angular momentum can be compensated by permanent re-excitations by continuous wave lasers which induce transitions from torsional to more excited intramolecular rotational states.

Acknowledgements

We are grateful to Dr. G.K. Paramonov (Minsk) for discussions of his approach [32] which may serve to maintain the unidirectional intramolecular motion in a dissipative environment. Financial support through a Grant-in-aid for Scientific Research (No. 1555002) from the Ministry of Education, Culture, Sports, Science and Technology of Japan (Y.F.) and through the Fonds der Industrie (J.M.) are acknowledged. The computations have been carried out in our HP 9000 machines at Berlin.

References

[1] K. Hoki, M. Yamaki, S. Koseki, Y. Fujimura, J. Chem. Phys. 118 (2003) 497.
[2] K. Hoki, M. Yamaki, Y. Fujimura, Angew. Chem. Int. Ed. 42 (2003) 2976.
[3] K. Hoki, M. Yamaki, S. Koseki, Y. Fujimura, J. Chem. Phys. 119 (2003) 12393.
[4] T.R. Kelly, H.D. Silva, R.A. Silva, Nature 401 (1999) 150.
[5] N. Koumura, R.W. Zijlstra, R.A. van Delden, N. Harada, B.L. Feringa, Nature 401 (1999) 152.
[6] B.L. Feringa, Acc. Chem. Res. 34 (2001) 504.
[7] R.A. van Delden, N. Koumura, A.M.A. Schoevaars, B.L. Feringa, Org. Biomol. Chem. 1 (2003) 33.
[8] J. Vacek, J. Michl, Proc. Natl. Acad. Sci. USA 98 (2001) 5481.
[9] L. Clarke, D. Horinek, G. Kottas, N. Varaksa, T. Magnera, T.P. Hinderer, R.D. Horanskz, J. Michl, J.G. Price, Nanotechnology 13 (2002) 533.
[10] J.-P. Sauvage, Molecular Machines and Motors, Springer, Berlin, 2001.
[11] J.-P. Sauvage, Acc. Chem. Res. 31 (1998) 611.
[12] J. Michl, T. Magnera, Proc. Nat. Acad. Sci. USA 99 (2002) 4788.
[13] T. Seideman, J. Phys. Condens. Matter (Topical Review Section) 15 (2003) R521.
[14] A.H. Zewail, Angew. Chem. Int. Ed. 39 (1999) 2586.
[15] S. Rice, M. Zhao, Optical Control of Molecular Dynamics, Wiley, New York, 2001.
[16] M. Shapiro, P. Brumer, Principles of the Quantum Control of Molecular Processes, Wiley, Hoboken, 2003.
[17] A. Assion, T. Baumert, M. Bergt, T. Brixner, B. Kiefer, V. Seyfried, M. Strehle, G. Gerber, Science 282 (1998) 919.
[18] N. Elghobashi, P. Krause, J. Manz, M. Oppel, Phys. Chem. Chem. Phys. 5 (2003) 4806.
[19] D. Kröner, L. González, Phys. Chem. Chem. Phys. 5 (2003) 3933.
[20] W.S. Knowles, Angew. Chem. Int. Ed. 41 (2001) 1998.
[21] R. Noyori, Angew. Chem. Int. Ed. 41 (2001) 2008.
[22] K.B. Sharpless, Angew. Chem. Int. Ed. 41 (2001) 2024.
[23] M.V. Korolkov, J. Manz, G.K. Paramonov, Adv. Chem. Phys. 101 (1997) 374.
[24] M.D. Feit, J.A. Fleck Jr., J. Chem. Phys. 78 (1983) 301.
[25] H. Kono, S.H. Lin, J. Chem. Phys. 84 (1986) 1071.
[26] A.D. Bandrauk, H. Shen, Can. J. Chem. 70 (1992) 555.
[27] A.D. Bandrauk, H. Shen, J. Chem. Phys. 99 (1993) 1185.
[28] J. Alvarellos, H. Metiu, J. Chem. Phys. 88 (1988) 4957.
[29] B. Schmidt et al., Wavepacket 3.0: a Program Package For Wavepacket Propagation and Time-Dependent Spectroscopy, Free University Berlin, Germany, 2003.
[30] C.C. Marston, G.G. Balint-Kurti, J. Chem. Phys. 91 (1989) 3571.
[31] D. Kröner, M.F. Shibl, L. González, Chem. Phys. Lett. 372 (2003) 242.
[32] M.V. Korolkov, G.K. Paramonov, Phys. Rev. A 55 (1997) 589.